



# Domination of volumetric toughening by silver nanoparticles over interfacial strengthening of carbon nanotubes in bactericidal hydroxyapatite biocomposite

Katharina Herkendell<sup>a,1</sup>, Vishnu Raj Shukla<sup>b,1</sup>, Anup Kumar Patel<sup>b</sup>, Kantesh Balani<sup>b,\*</sup>

<sup>a</sup> MVM – Department for Mechanical Process Engineering & Mechanics, Karlsruhe Institute of Technology, Germany

<sup>b</sup> Biomaterials Processing and Characterization Lab, Department of Materials Science and Engineering, Indian Institute of Technology Kanpur, India

## ARTICLE INFO

### Article history:

Received 13 July 2013

Received in revised form 11 September 2013

Accepted 28 September 2013

Available online 6 October 2013

### Keywords:

Hydroxyapatite (HA)

Silver (Ag)

Carbon nanotubes (CNTs)

Antibacterial

Cytocompatibility

Fracture toughness

## ABSTRACT

In order to address the problem of bacterial infections in bone-substitution surgery, it is essential that bone replacement biomaterials are equipped with bactericidal components. This research aims to optimize the content of silver (Ag), a well-known antibacterial metal, in a multiwalled carbon nanotube (CNT) reinforced hydroxyapatite (HA) composite, to yield a bioceramic which can be used as an antibacterial and tough surface of bone replacement prosthesis. The bactericidal properties evaluated using *Escherichia coli* and *Staphylococcus epidermidis* indicate that CNT reinforcement supports growth of Gram negative *E. coli* bacteria (~8.5% more adhesion than pure HA); but showed a strong decrease of Gram positive *S. epidermidis* bacteria (~diminished to 66%) compared to that of pure HA. Small amounts of silver (2–5 wt.%) already show a severe bactericidal effect when compared to that of HA–CNT (by 30% and ~60% respectively). MTT assay confirmed enhanced biocompatibility of L929 cells on HA–4 wt.% CNT (~121%), HA–4 wt.% CNT–1 wt.% Ag (~124%) sample and HA–4 wt.% CNT–2 wt.% Ag (~100%) when compared to that of pure HA. The samples with higher silver content showed decreased biocompatibility (77% for HA–4 wt.% CNT–5 wt.% Ag sample and 73% for HA–4 wt.% CNT–10 wt.% Ag). Though reinforcement of 4 wt.% CNT has shown an increase of fracture toughness by ~62%, silver reinforcement has shown enhancement of up to 244% (i.e. 3.43 times). Accordingly, isolation of toughening contribution indicates that volumetric toughening by silver dominates over interfacial strengthening contributed by CNTs towards enhanced fracture toughness of potential HA–Ag–CNT biocomposites.

© 2013 Elsevier B.V. All rights reserved.

## 1. Introduction

Hydroxyapatite (HA,  $\text{Ca}_{10}(\text{PO}_4)_6(\text{OH})_2$ ) is widely used in orthopedic surgery due to its similarity to apatite in human bone skeleton (Ca/P ratio 1.67), which displays an exceptional biocompatibility [1–3]. The poor hardness and fracture toughness and the promotion of bacterial growth, which leads to bacterial infection, are the two big challenges that are addressed in order to obviate implant rejection [4–7]. Carbon nanotube (CNT) reinforcement of HA has been widely studied to enhance the mechanical properties because of its high stiffness (Young's modulus of up to 1 TPa) [8–11]. Also CNTs are an attractive addition due to its physiochemical and biological properties [12–16]. Balani et al. and Agarwal et al. report superior optimized tribological and mechanical performance (fracture toughness increase of 56%) for HA–CNT composites containing 3–5 wt.% multiwalled CNTs, while showing good cytocompatibility [8,12]. The interaction of CNT with different bacteria

as well as mammalian cells is still being discussed controversially. The literature implies the dependence on various different factors like tube length and diameter, structure of the CNTs (multi- or singlewalled), functionalization of the CNTs, type of the cell and structure of the cell membrane (Gram positive/negative for bacteria). For mammalian cells, referring to bone forming, cell's multiwalled CNTs are reported to have good interaction with osteoblasts and fibroblasts [8–11,13,17–21], while depending on the size, singlewalled CNTs show cytotoxicity by blocking potassium channel activities and therefore might decrease the biocompatibility of implants [18,22].

Elimelech et al. has documented bactericidal properties for single- and multiwalled CNTs on *Escherichia coli* (Gram negative), eliciting severe bactericidal property of singlewalled CNTs due to the smaller diameter of the tubes [23]. Similar results exist for Gram positive and negative bacteria [24,25]. Then again, enhanced *E. coli* growth and proliferation on multiwalled CNTs are also reported in the literature [5]. To further handle the missing bactericidal properties of HA, several studies have been done on adding a second phase with antimicrobial agents [4,26–28]. Silver is a bactericidal metal with rising significance in biomedical applications [5,29]. It is known that  $\text{Ag}^+$  ions are able to diffuse into the cytoplasm through bacterial membranes, where they

\* Corresponding author. Tel.: +91 5122596194.

E-mail address: [kbalani@iitk.ac.in](mailto:kbalani@iitk.ac.in) (K. Balani).

<sup>1</sup> Have contributed equally as first authors.

interact with the DNA, RNA and bacterial enzymes, particularly to their SH-groups, leading to dysfunction of the cell metabolism and protein biosynthesis leading to suppression of cell division and ensued cell death [5,29–33]. Special attention has to be drawn on the influence of silver ions on human cells. Micrometer sized silver particles as well as silver nitrate or lactate are reported to show a strong cytotoxic effect which questions the application of silver in biocomposites [34]. On the other hand, recent studies demonstrate remaining biocompatibility upon addition of low amounts of silver nanoparticles [33,27]. Valiyaveetil et al. elaborated the mechanisms of AgNPs acting toxic on human fibroblast glioblastoma cells and stated a dependency of the cytotoxicity on the applied dose of AgNPs, making appearance by disruption of the mitochondrial respiratory chain of the cell, a reduced ATP content, increased production of reactive oxygen species and damaged DNA [35].

But, only a limited literature exists on simultaneously evaluating the effect of AgNPs on both, bacteria and mammalian cells that show antibacterial effects while retaining biocompatibility [27,33]. This indicates a different sensitivity towards a certain silver amount of eukaryotic and prokaryotic cells. Possible reasons are, for instance, differences in size and metabolic functions. Since eukaryotic cells are usually larger than prokaryotic cells, a far bigger concentration of silver ions is necessary to achieve a similar toxic effect. Also, high structural organization of eukaryotic cells through compartmentalization, which enables decentralized energy conservation in mitochondria or the separated DNA localization in the core, weakens the impact of silver ions compared to prokaryotes [33]. Referring to silver reinforced implants this observation suggests that an AgNP dose range can be found, in which prokaryotic cell metabolism is successfully hampered, while no constraint eukaryotic viability can yet be observed.

To achieve densification of novel materials, spark plasma sintering (SPS) has been established over the last decades, evolving from the idea of activating the sintering process by the use of electrical current that was introduced in 1933 [36]. Evident advantages compared to conventional methods like pressureless sintering or hot pressing reside in decreased sintering temperature (by 150–200 °C) and shortened dwell times (sintering time of 5–15 min). These innovations allow sintering of nanometer-sized powders to near theoretical values with sparse grain growth [36–38]. The high densification of the powder sample obtained by sintering via the SPS route is favorable for the enhanced mechanical properties of the composite. Still, CNTs tend to cluster and entangle during sintering, which can lead to marginally higher porosity of the sample [5]. At moderate sintering temperatures of 900–1200 °C, decomposition of HA with formation of a TCP phase (at 1400 °C) [7,39] and the carbon nanotubes in spheroid particles at temperatures higher than 1700 °C can be avoided [5,40–43].

For samples containing silver which has a melting point of ~960 °C, sintering can bear the benefit of densification through a liquid silver phase, but de-mixing of the phases needs to be avoided [5]. Functionally graded materials are a new approach to meet the requirements of bioceramics to interact best possible with the surrounding tissue and still bear the high hardness and fracture toughness in the core to handle the loads of a long lasting implant. In a non-monolithic bone replacement material, highly bioactive components like reinforced HA on the outside can be combined with inner layers of strong materials like yttria stabilized zirconia or alumina oxide [44]. Challenges are to durably bond the different layers to a single composite which means that a high gradient of mechanical properties is not favorable. It has been shown, that the implication of intermediate layers with adjusted qualities can lead to a gradual change among properties from surface to core, and therefore elicit reliable mechanical performance [44–47].

The main focus of the present study is the enhancement of antibacterial properties with the highest possible content of silver without influencing the good attachment of body cells and without decreasing the mechanical properties. In regard to the application of HA–CNT–Ag, as a part of functionally graded material, HA is reinforced with 4 wt.% of multiwalled carbon nanotubes to improve the mechanical strength and

to make it compatible with potential other layers. The CNT reinforced HA matrix is complemented by a varying silver-nanoparticle content of 0; 1; 2; 5 and 10 wt.%. The influence of the mechanical properties is characterized by Vickers indentation and indentation fracture toughness. Pure HA is processed under the same conditions and is used as a reference. Bactericidal properties are evaluated using Gram positive (*Staphylococcus epidermidis*) as well as Gram negative (*E. coli*) bacterial colonies. In order to establish the optimal content of silver, cytocompatibility of sintered HA–CNT–Ag biocomposites is studied though *in vitro* cell culture with L929 mouse fibroblast cell line, which is quantified via MTT assay.

## 2. Materials and methods

### 2.1. Material processing

Starting powders were hydroxyapatite (HA), multiwalled carbon nanotubes (CNTs) and silver nanoparticles (AgNPs). HA powder (~15–55 nm) was synthesized using a suspension-precipitation method [5,10] and it was ball-milled for 16 h with a ball-mass ratio of 10:1 in ethanol. Multiwalled CNTs (95% purity, inner dia 20 nm, and outer dia 40 nm, 1–2 µm long) were purchased from Nanostructured & Amorphous Materials Inc., United States. The dried HA powder and the CNTs were sieved separately for homogenization with a sieve of mesh size 120 (125 µm). The AgNPs were procured from Sigma Aldrich, United States, with high purity (99.5%) and with particle size of less than 100 nm. Powder mixtures of six different compositions were prepared which were pure HA, HA with 4 wt.% CNT, HA with 4 wt.% CNT and x wt.% AgNPs where x = 1, 2, 5 and 10. The nomenclature of the prepared powders is provided in Table 1. The SEM image of powder mixture of HA with 4 wt.% CNT and 10 wt.% Ag has been shown in Fig. 1(a). The powders were mixed in ethanol and ultrasonicated for 5 min followed by magnetic stirring while heating at 80 °C in order to evaporate the solvent. This obtained paste was dried for 12 h at 200 °C and subsequently sieved with mesh size 170 (90 µm). Quantitative elemental analysis, Fig. 1(b), shows the presence of silver in HA–CNT matrix.

The powders were subsequently processed by rapid spark plasma sintering (SPS, Dr. Sinter 1050 SPS apparatus, Sumitomo, Japan/Dr. Sinter 511 S SPS) in a cylindrical graphite die with an inner diameter of 15 mm. Sintering was performed at temperature of 950 °C (with ramp rate of 100 °C/min) and a dwell time of 5 min under uniaxial pressure of 30 MPa in vacuum (~6 Pa) in order to obtain dense ~3 mm thick pellets.

### 2.2. Phase and microstructural characterization

The density of the pellets was measured via Archimedes' water immersion principal using distilled water on a commercial weighing machine (Citizen CX 220) with decimal accuracy of 0.1 mg. The theoretical densities of the composites while taking the density of pure component were taken as 3.16 g cm<sup>-3</sup>, 2.10 g cm<sup>-3</sup>, 10.49 g cm<sup>-3</sup> and 0.988 g cm<sup>-3</sup> for HA, CNT, Ag and H<sub>2</sub>O respectively. Porosity may affect cell adhesion due to affected roughness and enhanced surface area [48].

The pellets were polished with emery paper followed by cloth polishing with an alumina particle suspension, particle size 5 µm and 1 µm. Phase analysis was conducted with X-ray diffraction technique (X-ray diffraction; ISO Debyelex-2002, Rich Seifert & Co., Germany) with CuK<sub>α</sub> radiation, λ = 0.15418 nm at a step size of 0.02°, and scan rate of 1°/min. The critical analysis of the X-ray diffraction-data for confirming phase stability and absence of undesirable formed products during sintering was performed with the help of Pearson's Crystal Data Base (PCD). Raman spectroscopy (WITec GmbH, Germany, alpha 300 series microscope equipped with a furnace cooled charge coupled device (CCD)) was performed on the samples to detect the presence of CNT using argon laser (of wavelength of 514 nm).

The fractured surfaces and distribution of the CNTs and Ag were examined via scanning electron microscopy (SEM; SUPRA 40VP, Carl Zeiss NTS GmbH, Germany), and elemental analysis was carried out using

**Table 1**  
Composition, e-modulus and density of HA–Ag–CNT sintered samples.

Sample	Composition	E-modulus (theoretical) [GPa]	Density (theoretical) (g/cm <sup>3</sup> )	Density (Archimedes) (g/cm <sup>3</sup> )	% relative theoretical density
COA0	100 wt.% HA	110.0	3.16	2.98	94.5
C4A0	96 wt.% HA + 4 wt.% CNT	156.6	3.09	2.97	95.9
C4A1	95 wt.% HA + 4 wt.% CNT + 1 wt.% Ag	156.8	3.12	2.95	94.7
C4A2	94 wt.% HA + 4 wt.% CNT + 2 wt.% Ag	157.0	3.14	3.01	95.8
C4A5	91 wt.% HA + 4 wt.% CNT + 5 wt.% Ag	157.8	3.20	3.07	95.9
C4A10	86 wt.% HA + 4 wt.% CNT + 10 wt.% Ag	159.1	3.32	3.17	95.5

energy dispersive spectroscopy (EDS, OXFORD Instrument, INCA Penta FETx3).

### 2.3. Mechanical property evaluation

Hardness of sintered samples was calculated via Vickers indentation at 200 g load with a dwell time of 10 s using a Vickers automat (V-Test, Bareiss Prüfgerätebau GmbH, Germany). Whereas, the fracture toughness ( $K_{IC}$ ) was determined via Anstis' equation [49]:

$$K_{IC} = 0.016(E/H)^{1/2} * F/c^{3/2} \quad (1)$$

where E = elastic modulus, H = Vickers hardness, F = applied load and c = crack length from the center of the indent. In order to generate an indent crack, Vickers indentation was performed at a load of 2 kg (dwell time of 10 s) for evaluating fracture toughness. Exact estimation of the crack length was obtained using SEM observations. The theoretical elastic modulus (E) was determined by the rule of mixtures using the volume percentage of the pure components. Their theoretical Young's moduli were taken to be 110 GPa, 900 GPa [50] and 83 GPa for HA, CNT and Ag respectively.

### 2.4. Estimation of bactericidal property of processed HA–CNT–Ag composites

The antimicrobial tests were conducted with *E. coli* (ATCC #25922) to evaluate the bactericidal properties against Gram-negative bacteria and with *S. epidermidis* (ATCC #35984) for Gram-positive bacteria. The polished samples were ultrasonicated for 20 min, autoclaved and placed in a 24-well plate. After sterilizing the samples under UV light for 30 min, each sample was immersed in ethanol for 1 h and washed twice with PBS (15 min). For bacterial studies, COA0 sample was used as control sample. The seeding was done using 100  $\mu$ L of 0.1 optical density bacteria solution (*E. coli*, *S. epidermidis*). A 700  $\mu$ L solution of fresh Luria Broth (LB) media was added in the well plate, and was incubated

for 4 h at  $37.4 \pm 0.6$  °C. Washing was done with  $1 \times$  PBS, 3% glutaraldehyde (20 min), 0.1 M sodium cacodylate (15 min) and 0.1 M sucrose (15 min). Dehydration was done with two 10 min dipping in different ethanol solutions (30; 50; 70; 95; 100%) and for the final step using the critical point dryer hexamethyldisilazane (HMDS). The samples were sputter-coated with gold nanoparticles and then watched under SEM to observe and count the bacterial attachment. The experiment was repeated twice with each bacterial type. Student *t*-test was performed to check the null-hypothesis, and confirm the statistical difference between the average values of bacterial counts with p value of <0.05 at a confidence level of greater than 95%.

### 2.5. Cytocompatibility of spark plasma sintered HA–CNT–Ag composites

In order to evaluate the influence of the silver content on the adhesion of surrounding tissue to the biocomposite, a cell culture study with L929 mouse fibroblasts was performed. Since fibroblasts are widely accepted as representative cells for biocompatibility testing, their low specialization, uncomplicated replication in-vitro and standardized culture conditions provide suitable conditions for reproducible and comparable results.

Parallely, in vivo fibroblasts are the most occurring mammalian cells of the connecting tissue, and their synthesis of extra cellular matrix is essential in wound healing and therefore enables other cell types to connect with foreign material. Hence, their scan of a surface gives valuable information by cell signaling to e.g. osteoblast cells, which are responsible for new bone formation. This means that the interaction of fibroblasts and foreign material enables tissue growth and therefore is an important indicator for the cytocompatibility of implants. Thus, in order to affect the cytocompatibility, L929 mouse fibroblasts were used in this study.

About 3 mm  $\times$  3 mm pieces of the polished samples were ultrasonicated for 20 min, autoclaved and placed in 24 well plate where they were sterilized under UV light for 30 min. Then the samples were dipped in 70% ethanol for 20 min and washed with  $1 \times$  PBS. A glass

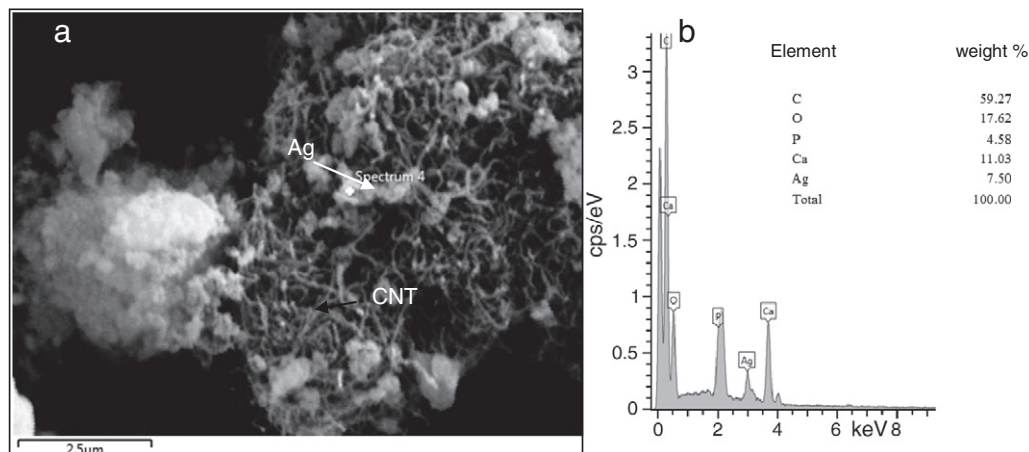


**Fig. 1.** (a) A selected portion of C4A10 composition powder prepared for SPS. (b) Quantitative elemental analysis of region showing the presence of silver.

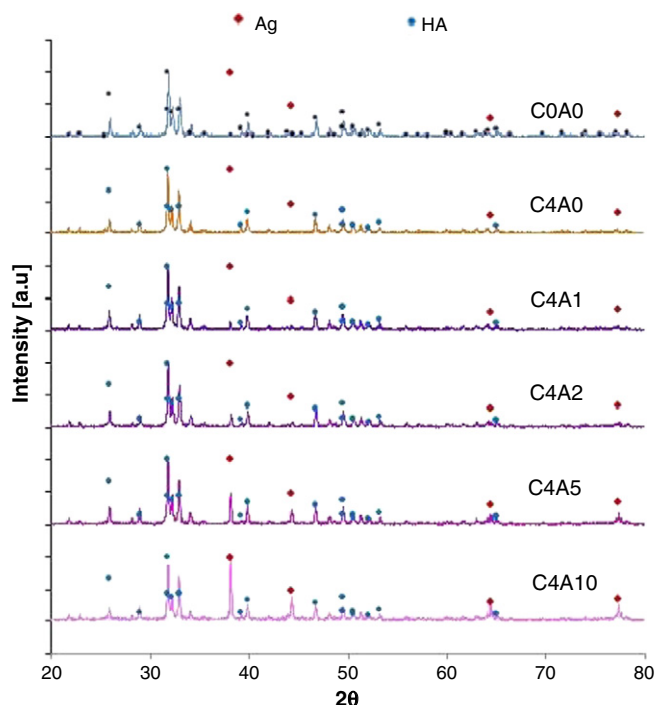


Fig. 2. Intensity vs.  $2\theta$  curve for X-ray diffraction of the spark plasma HA–CNT–Ag samples.

cover slip coated with 0.2% gelatin was used as a control sample. The stock solution was prepared with metabolically highly active cells in Dulbecco's modified Eagle's medium (DMEM). The seeding was done at  $200 \mu\text{L}$  of  $5 \times 10^4$  cells/mL solution. Further,  $200 \mu\text{L}$  of fresh media was added and the well plate was incubated for  $72 \text{ h}$  at  $37.4 \pm 0.6^\circ\text{C}$ . Washing was done with  $1 \times \text{PBS}$ , 2% glutaraldehyde (20 min) and again  $1 \times \text{PBS}$ . Dehydration was done for 10 min each dipping in different ethanol solutions (30; 50; 70; 90; 100%) and final step using the critical point dryer HMDS.

For the semi-quantitative analysis of the cell viability an MTT (3-(4,5-dimethylthiazol-2-yl)-2,5-diphenyl tetrazolium bromide) assay after the method of Mosmann was done. After 72 h of incubation, the samples were washed twice with PBS, then  $10 \mu\text{L}$  of MTT was added to each well

through  $100 \mu\text{L}$  DMEM with 5 mg MTT per mL PBS. After incubation for 4 h and precipitation of formazan crystals through reaction of MTT with the L929 mitochondria, the media were aspirated and the crystals were dissolved in  $200 \mu\text{L}$  of dimethyl sulfoxide (DMSO) giving a purple solution. The solutions were transferred into a 96 well plate and the optical density was determined by a microplate reader (Automated Microplate Reader, Bio/Tek, model ELx800) at 490 nm with DMSO as blank sample. Student *t*-test was performed to check the null-hypothesis, and confirm the statistical difference between the average optical density of L929 cells with a value of  $<0.05$  at a confidence level of greater than 95%.

### 3. Results and discussions

#### 3.1. Phase analysis of HA–CNT–Ag samples

##### 3.1.1. X-ray diffraction

The X-ray diffraction profiles of the sintered samples of pure HA (C0A0) and HA with 4 wt.% CNT and varying silver content (C4A (1/2/5/10)) are shown in Fig. 2. All characteristic peaks of HA were identified, and the absence of additional peaks implies that no decomposition of the initial powders has taken place. Particularly, formation of  $\beta$ -TCP (tricalcium phosphate) has not occurred during the sintering process, which can be attributed to the low sintering temperature ( $950^\circ\text{C}$ ) and short processing time (5 min) incurred during spark plasma sintering. The increasing silver content from sample C4A0 to C4A10 can strongly be observed in the increased intensity of the corresponding Ag peaks of (111), (200), (220) and (311) with  $2\theta$  of  $38.08^\circ$ ;  $44.26^\circ$ ;  $64.38^\circ$  and  $77.32^\circ$ , respectively. Peaks of graphite, which match best the carbon structure in CNTs, are not being observed in the composites owing to feeble intensity of the peaks. Since the CNT ratio is only 4 wt.%, the most significant peak at  $2\theta = 26.38^\circ$  is getting shadowed by the presence of HA ( $2\theta = 25.84^\circ$ ).

##### 3.1.2. Raman spectroscopy

The Raman spectra of the SPS samples are presented in Fig. 3. A non-dissociated HA-phase is reconfirmed by the presence of the characteristic peaks at  $429$ ,  $590$ ,  $958$  and  $1045 \text{ cm}^{-1}$ , which indicate the stretching of different bonds in  $\text{PO}_4^{3-}$  ions. The most intense peak at  $958 \text{ cm}^{-1}$  corresponds to the symmetrical stretching of the tetrahedron of oxygen atoms, surrounding the phosphorus atom, confirming the presence of undissociated HA [51,52]. The retention of undamaged CNTs is also

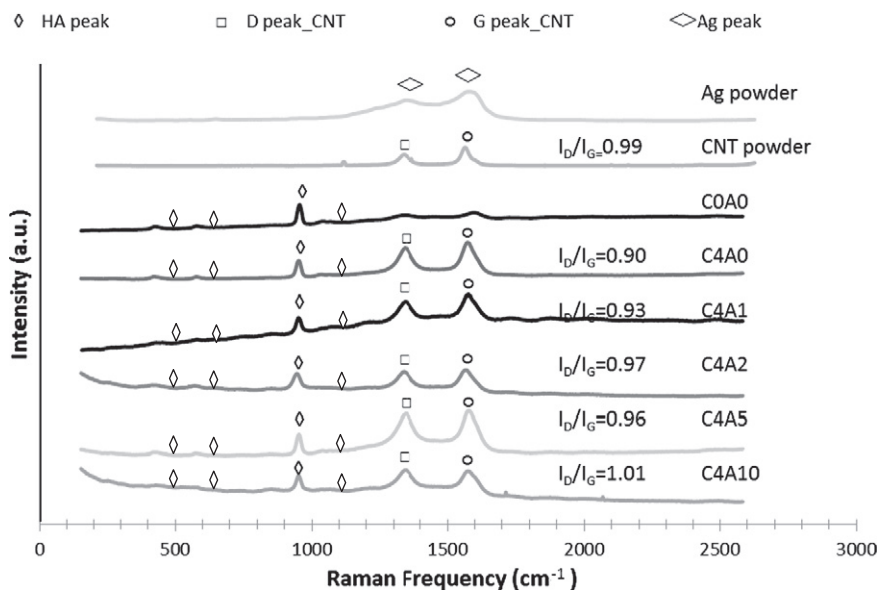


Fig. 3. Raman spectrum eliciting retention of CNTs even after spark plasma sintering of A–CNT–Ag samples.

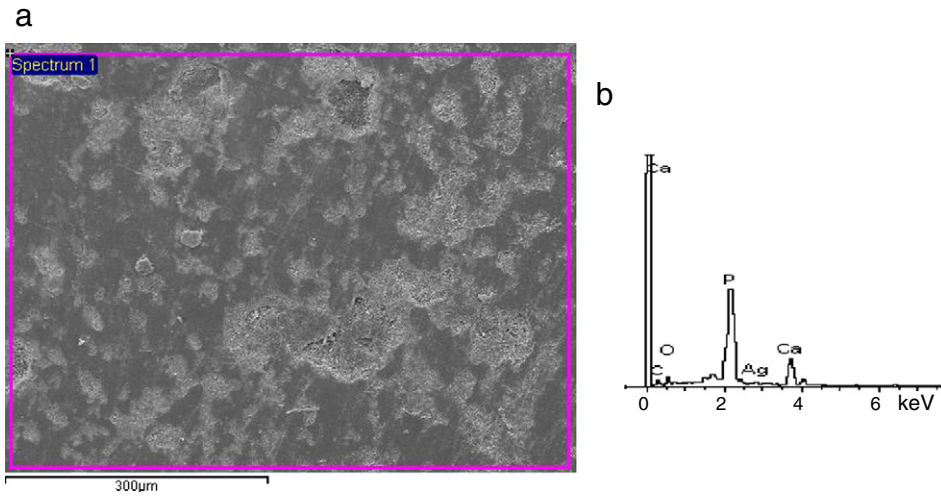


Fig. 4. (a) EDS of selected area of C4A5 sintered pellet (b) elemental analysis of selected area showing presence of Ag in HA matrix.

confirmed for all SPSeD samples, viz. (C4A0, C4A1, C4A2, C4A5, C4A10) from the presence of distinctive G-peaks at  $1580\text{ cm}^{-1}$  and D-peaks at  $1350\text{ cm}^{-1}$  as shown in Fig. 3. The G-band is a high-frequency  $E_{2g}$  first-order mode from graphite-like  $sp^2$  type bonds [53,54], whereas disorders or defects of the graphitic layers are indicated by the intensity of the D-band due to activation of diamond like  $sp^3$  bonds [53,55]. The intensity ratio ( $I_D/I_G$ ) of both bands is 0.90–1.01 for all compositions which is concurrent with the values for starting multiwalled CNTs. It can be concluded that no structural changes have occurred during sintering and that the degree of defects in the graphitic phase is not higher than in pure CNT

powder [5,54,55]. A peak at  $1100\text{ cm}^{-1}$  in pure CNT is attributed to C–O stretching in CNTs. This functionalization (of C–O) may have occurred because of CNTs interacting with the ethanol used for washing the CNTs.

### 3.2. Microstructural characterization

The SEM image of the SPSeD pellet of composition HA–4 wt.% CNT–5 wt.% Ag and its quantitative elemental analysis has been

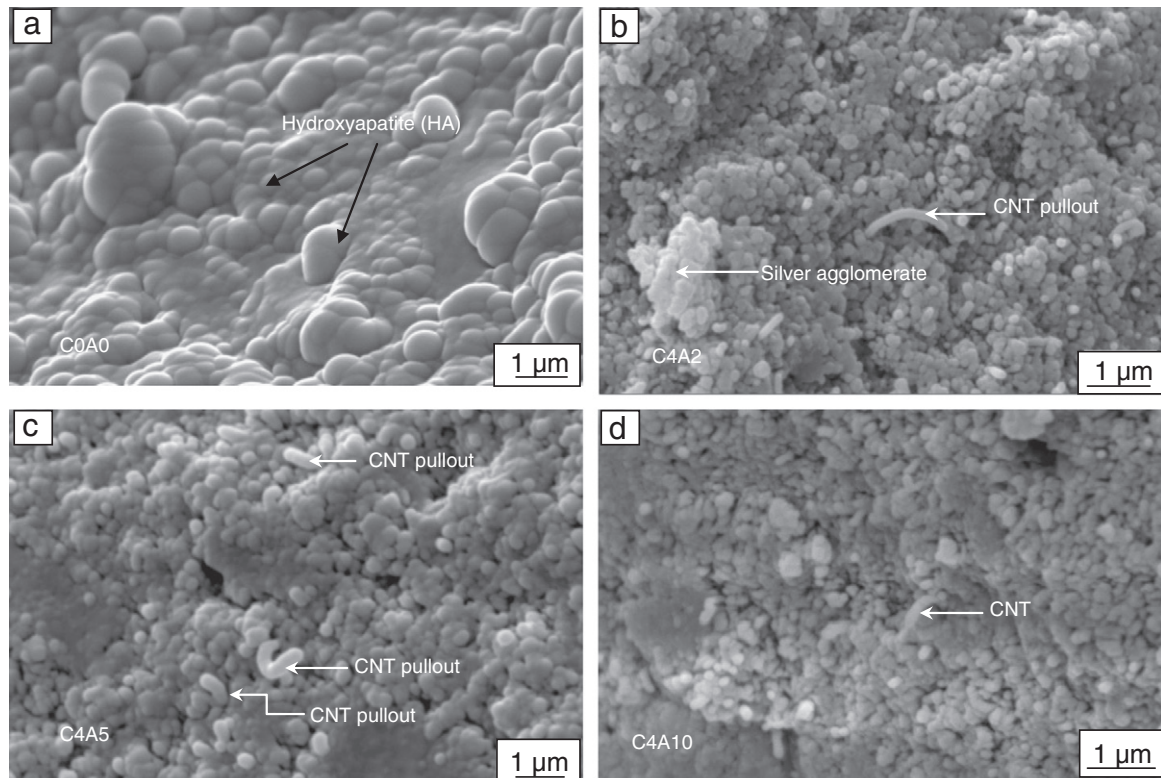


Fig. 5. Fractured surfaces of pellets (a) C0A0, (b) C4A2, (c) C4A5, (d) C4A10 showing grain size variation and CNT-pullout in CNT reinforced pellets.

shown in Fig. 4(a) and (b), respectively. The elemental analysis shows the presence of silver and carbon.

Fig. 5 shows SEM images of fractured surfaces of samples processed using SPS at a temperature of 950 °C and a dwell time of 5 min which ensured a high densification of the samples. The density of the samples, evaluated by Archimedes immersion principle, shows over 94.5% relative theoretical densification. As expected, the densities of C4A5 and C4A10 were significantly higher than other samples, which is attributed to

lower melting point (~960 °C) of Ag. All samples, SPS sintered samples, are 94.5–96% dense.

Grain size in C0A0 sample is ~0.5 µm, whereas when HA is reinforced with CNT and Ag, the grain size decreases down to less than 0.2 µm as shown in the fractured surfaces of C4A2, C4A5 and C4A10 (Fig. 5). Apparently, the HA, CNT and Ag nanoparticles seem to be retained homogeneously in the samples even after SPS (confirmed via EDS, but not shown here). A marginal agglomeration of silver is also observed

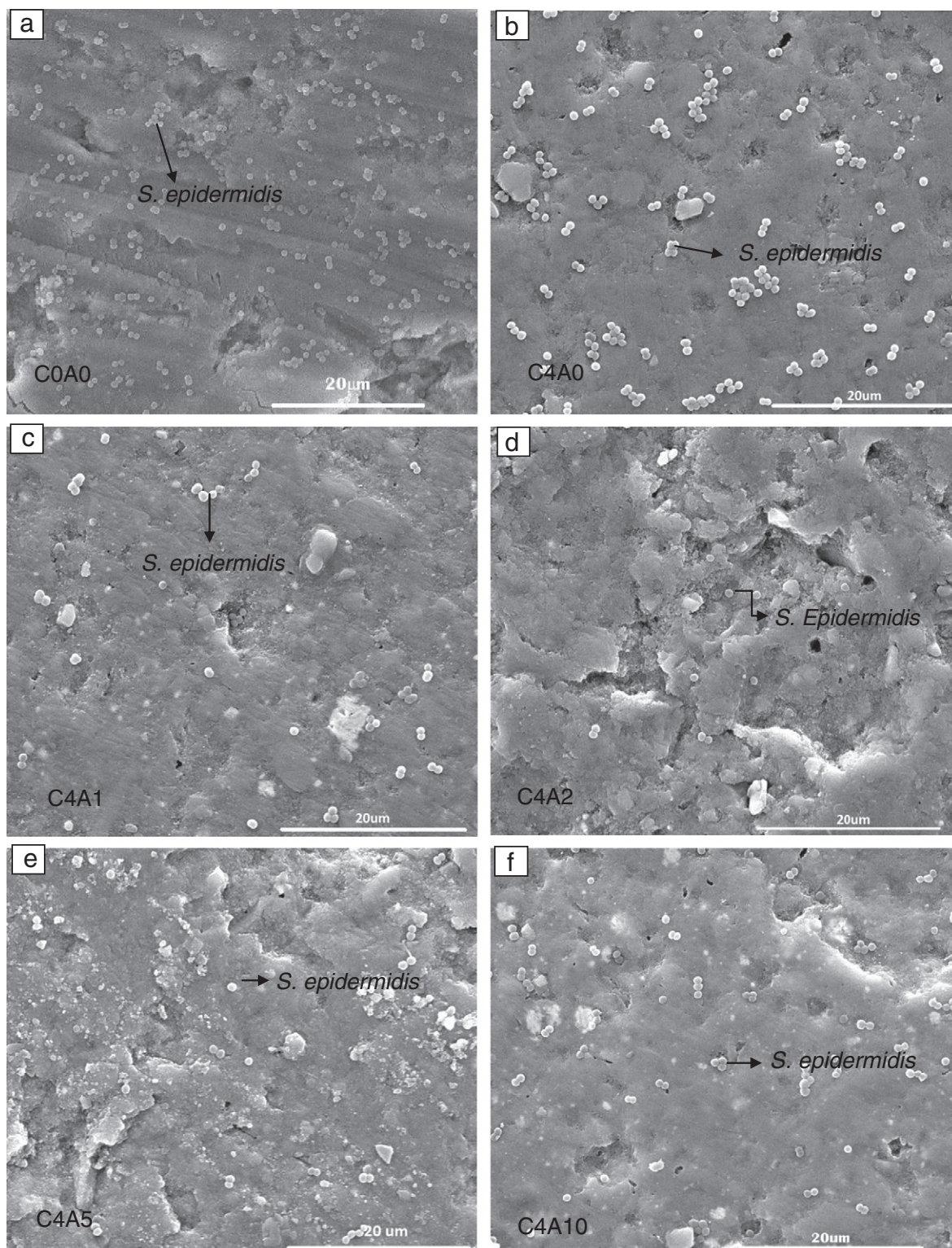


Fig. 6. SEM images of *S. epidermidis* bacteria cultured on samples (a) C0A0, (b) C4A0, (c) C4A1, (d) C4A2, (e) C4A5, (f) C4A10.

in the samples (Fig. 5b). Apparently, breakage of CNT, as CNT-pullout, can be observed in the C4A2 and C4A5 samples (Fig. 5c and d) which is expected to toughen the matrix [56,57].

### 3.3. Antibacterial properties

#### 3.3.1. Role of Ag in affecting *S. epidermidis* bacterial atrophy

Fig. 6 shows SEM images of *S. epidermidis* bacteria adhered to the sample surfaces of different compositions after culturing for 4 h. For morphological comparison, pure hydroxyapatite (C0A0) was utilized as the base sample, and experiment was repeated three times to obtain the average values. Spheroid shaped bacteria are visible on the surfaces of all the samples. There is a sharp decrease in the number of bacterial colonies moving from C0A0 over C4A0 to the silver reinforced samples (C4Ax). A bactericidal effect of CNTs on the Gram positive bacteria can be deduced comparing Fig. 6(a) and (b). High bacterial count on C0A0 and C4A0 shows that hydroxyapatite and CNT are prone to bacterial infection.

As the content of silver increases, there is a further decrease in the colonies and the bacterial count attributed to the bactericidal property of silver. A strongly diminished number of microbes are observed to be in pairs or groups of more in samples C4A1 and C4A2 (Fig. 6(c) and (d)); even more distinctly visible for C4A5 and C4A10 (Fig. 6(e) and (f)) suggesting a strong slowing down in the ongoing process of cell proliferation which is obviously being suppressed by AgNPs.

The cell count of the *S. epidermidis* culture is recorded in Fig. 7 along with error bars showing the standard deviation, confirming a decrease by around 34% upon CNT addition. The bacterial count on C4A1 and C4A2 is not significantly different. The C4A5 and C4A10 samples behave similarly against *S. epidermidis* since the counts are not statistically significantly different as suggested by *t*-test. The mechanism of AgNPs inhibiting bacterial metabolism and proliferation through denaturation of DNA and structural change of enzymes is described in a study by Afzal et al. [5].

#### 3.3.2. Role of Ag in affecting *E. coli* bacterial atrophy

Similar to *S. epidermidis*, after the four hour incubation of *E. coli* on the surfaces of all compositions, the cell growth can be observe via SEM imaging (Fig. 8). The experiment has been repeated three times to obtain the average values. *Bacillus* shaped bacteria are observed on the surface of the HA (Fig. 8a), and with CNT (Fig. 8b) addition. Both surfaces show a very high growth of the Gram negative bacteria, suggesting a high bacterial density in the initial cell suspension for inoculation. Furthermore, large colonies of *E. coli* in C4A0 sample suggest highly supportive properties for growth and proliferation of *E. coli* (Fig. 8b). But, with increasing silver content, a decrease in bacterial count can be observed (Fig. 8c–f). A decrease in the colonies and the bacterial count with increasing silver content is attributed to the bactericidal property of silver.

Quantification of bacteria on the surfaces of HA–CNT–Ag samples is presented in Fig. 9. Unlike *S. epidermidis*, CNT seems to support *E. coli* proliferation, giving an 8.58% higher cell growth on C4A0 than C0A0 (reference sample). For all amounts of silver, a decrease in bacterial adhesion can be observed. Bacterial count is significantly lower in pure HA with an average of 76.8, 58.7, 50.8 and 35.3% for C4A1, C4A2, C4A5 and C4A10, respectively. But, it can be noted that the difference of bacterial count is not significantly different for C4A2 compared to C4A5 sample. In general, this study confirms the conclusion that AgNPs decelerate *E. coli* growth and division.

Strong bactericidal property of Ag is attributed to the formation of complexes and denaturing of DNA by silver ions [5]. Such bactericidal effect of Ag, on both Gram positive *S. epidermidis* and Gram negative *E. coli*, is also observed by various researchers [5].

### 3.4. Cytocompatibility

The cell viability testing after a three day culture of mouse fibroblasts on the pellets of six different compositions was done using the MTT assay. As a seventh sample gelatin coated glass cover slip served as control, taking the optical density of its assay as the standard for 100% cell viability. MTT assay test was performed on HA–CNT–Ag samples three times with two samples of each kind in the test. An average of cell density is reported in Fig. 10.

Highly dense sintered pure HA (C0A0) appears to have similar cell viability as the control sample (99%), stating an excellent biocompatibility of HA. Upon CNT addition (C4A0) a significant increase (21% higher) in cell viability implies an advantageous function of the multiwalled CNTs for cell attachment and survival when compared to base HA sample. The sample with 1 wt.% silver C4A1 shows slightly increased cell viability (23.8% more than control), whereas C4A2 shows decrease in values compared to C4A1 but still shows the same cell viability as that of pure HA (C4A0) and the control surface. It can be deduced that the synergy of the cell supporting effect of 4 wt.% CNT and the cell diminishing effect of 2 wt.% AgNPs nullifies each other (in C4A2 sample). The amount of vital cells is 76.7% for HA–C4A5 and 72.5% for C4A10 compared to pure HA.

The cell cycle of L929 fibroblasts in standard culture conditions is around 24 h [58]. Thus, depending on the needed time for adhesion and the initial cycle phase of the cells during the inoculation, a metabolically active cell can divide between zero and three times in 72 h. Hence, the results of the 3 day–MTT assay predominantly gives an insight into the first response (indicating the ability to adhere and acclimatize to the new environment) of fibroblasts against the surfaces of different compositions [10]. It is assumed that the presence of silver severely perturbs the cell metabolism, hampering the respiratory chain and therefore obviating adhesion, growth and proliferation, leading to diminished bacterial viability [35].

A comparative representation of bacterial and osteoblast cell activity (Fig. 11) elicits that CNT reinforcement increased the L929 mouse fibroblast cell viability and *E. coli* bacterial density appreciably, whereas *S. epidermidis* bacterial count shows a decrease. Thus, CNTs seem to be cytocompatible for L929 fibroblast cells and Gram positive bacteria. But, cell and bacterial density is observed to decrease upon addition of more than 1 wt.% Ag which is attributed to bactericidal effect of silver. The L929 cell viability of C4A1 sample is increased by more than a quarter times with respect to pure HA (C0A0), whereas the cell viability of C4A2 is the same as that of pure HA (C0A0). On addition of 5 wt.% Ag, the L929 cell viability decreases to 77% of that of pure HA. Further, *E. coli* bacterial count is seen to be two thirds of cell count on C0A0 for

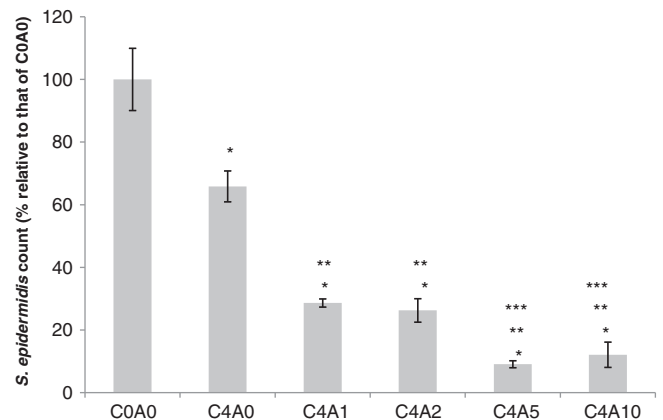


Fig. 7. *S. epidermidis* cell density on the spark plasma sintered HA–CNT–Ag samples. \* means that there is a significant difference in the bacterial counts as compared to C0A0. \*\* means that there is a significant difference in the bacterial counts as compared to C4A0. \*\*\* means that there is a significant difference in the bacterial counts as compared to C4A1 and C4A2. In all the cases  $p < 0.002$ .

C4A1 sample. C4A2 sample shows even less *E. coli* bacterial count, i.e. 53% of cell count on C0A0 sample. *S. epidermidis* is only 28% and 22% of that on C0A0. It is therefore expected that a silver content of 2–10 wt.% along with 4 wt.% CNT in HA will give optimized cytocompatibility and bactericidal effect.

In consideration of *E. coli* (being a Gram-negative bacteria) and *S. epidermidis* (being a Gram-positive bacteria) response against the sintered HA–CNT–Ag composites, the contrasting behavior is attributed to different typology of the cell-envelope. As illustrated in Fig. 11, the cell envelope of Gram-negative bacteria consists of two lipid membranes

and a thin embedded peptidoglycan layer ( $\approx 10$  nm). On the other hand Gram-positive bacterial cell envelopes contain just one lipid membrane and a much thicker peptidoglycan layer of up to 80 nm with accumulated surface proteins. Fibroblasts as mammalian cells have a double layer lipid membrane serving as the separation from extracellular space and cytoplasm. Since the results show enhanced fibroblast viability, even upon CNT addition, it is quite likely that multi-walled CNTs interact with the surface protein layer and peptidoglycans in a way that retains cell adherence, but diminishes the growth of Gram negative bacteria due to easy complex formation with its nuclei. The bactericidal properties

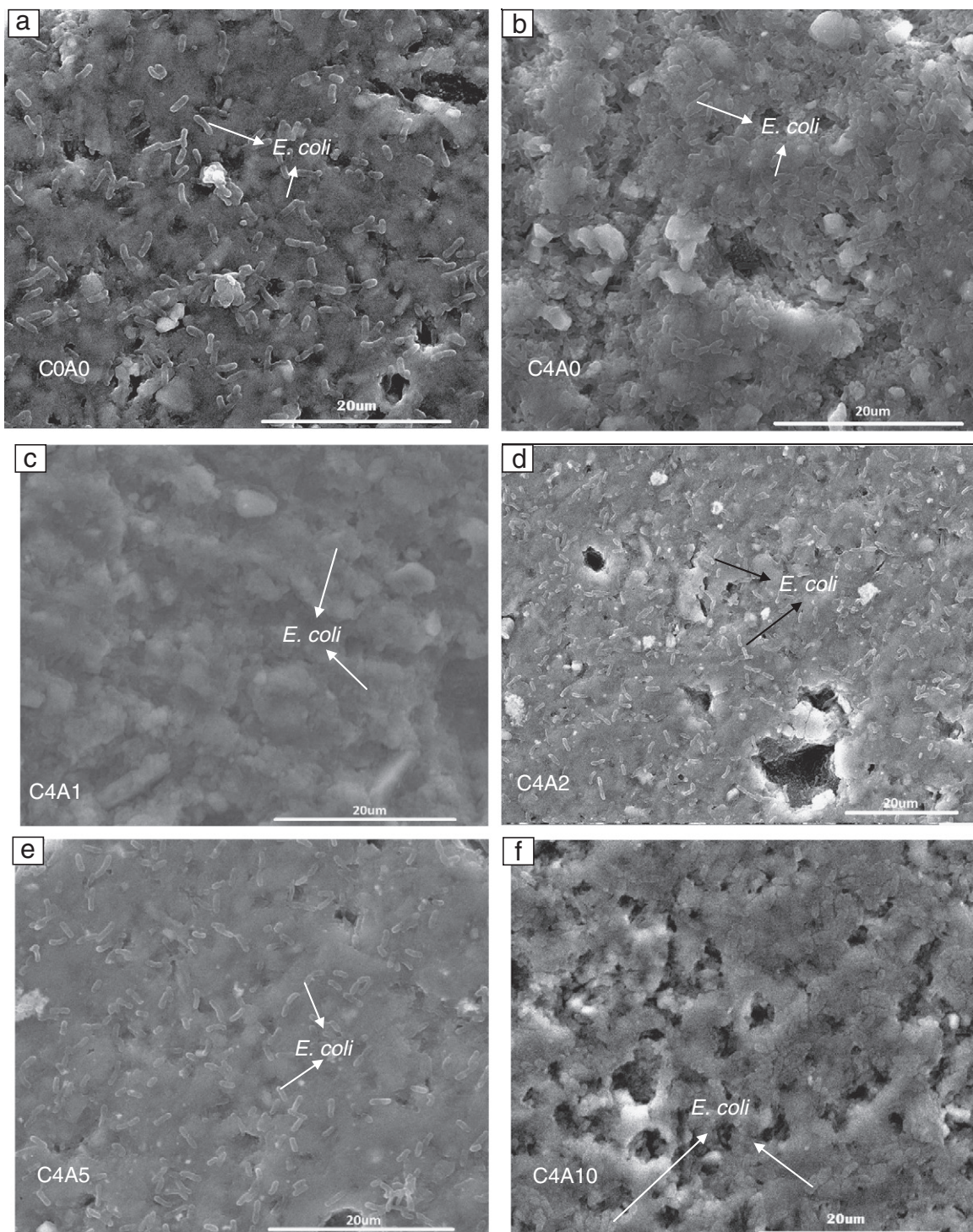


Fig. 8. SEM image of *E. coli* bacterial culture on samples (a) C0A0, (b) C4A0, (c) C4A1, (d) C4A2, (e) C4A5, (f) C4A10.

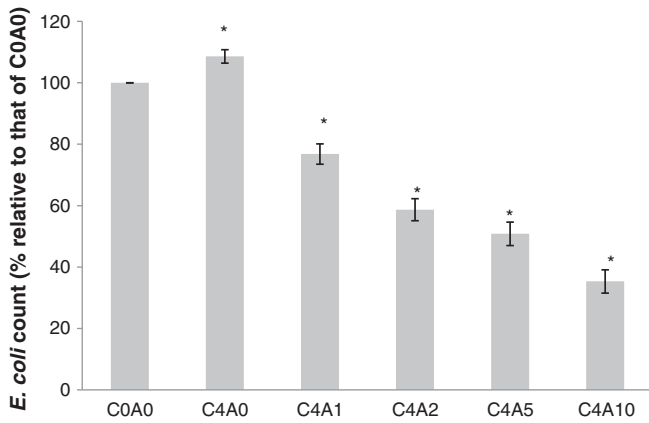


Fig. 9. *E. coli* cell density on the samples. \* means that the bacterial count is significantly different from that on C0A0. In all cases  $p < 0.0003$ .

of silver nanoparticles are evident in Figs. 6–9. According to the expectations, a strong decrease in bacterial viability can be observed with increasing silver concentration for *E. coli* as well as *S. epidermidis* as mentioned before.

The differential shift of about 0.4 between the response against *E. coli* and *S. epidermidis* is considered to apply to all samples. Incorporating this shift, all Ag containing samples also appear to show similar decrease in bacterial attachment with increasing silver concentrations. Such a trend substantiates that Ag<sup>+</sup> ion invasion is independent of cell-envelope structure and that a strong inhibition of cell growth is attested for both, Gram-positive and Gram-negative bacteria with decreasing cytocompatibility. Once the silver ions have overcome the bacterial membranes by diffusion through transmembrane proteins like porins, they have direct access to the DNA floating in the cytoplasm. Also all kinds of enzymes, ribosomes and RNA which are essential for the bacteria's metabolism are unprotected, giving smallest amounts of silver ion's various locations to cause severe damage. That is the reason that such a decreasing trend is attained even with small amounts of silver concentrations (1–2 wt.%). It is indicated in the literature that Ag<sup>+</sup> ions are able to diffuse into the cytoplasm through bacterial membranes, where they interact with the DNA and RNA and bind to bacterial enzymes, particularly to their SH-groups, leading to dysfunction of the bacteria's metabolism and protein biosynthesis leading to suppression of cell division and subsequent cell death [5,59–63].

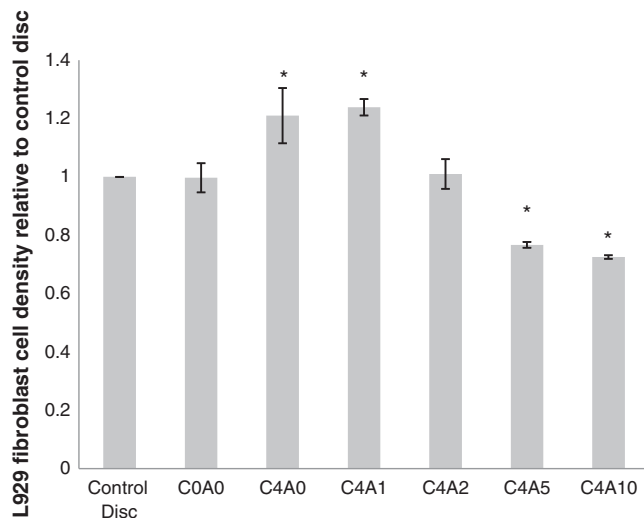


Fig. 10. L929 fibroblast cell densities on the samples after 3-day culture. \* means that the cell count is significantly different from that on control sample, with  $p < 0.02$ .

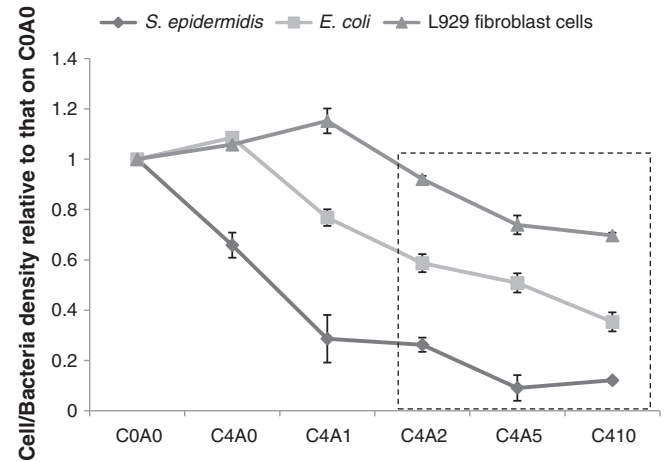
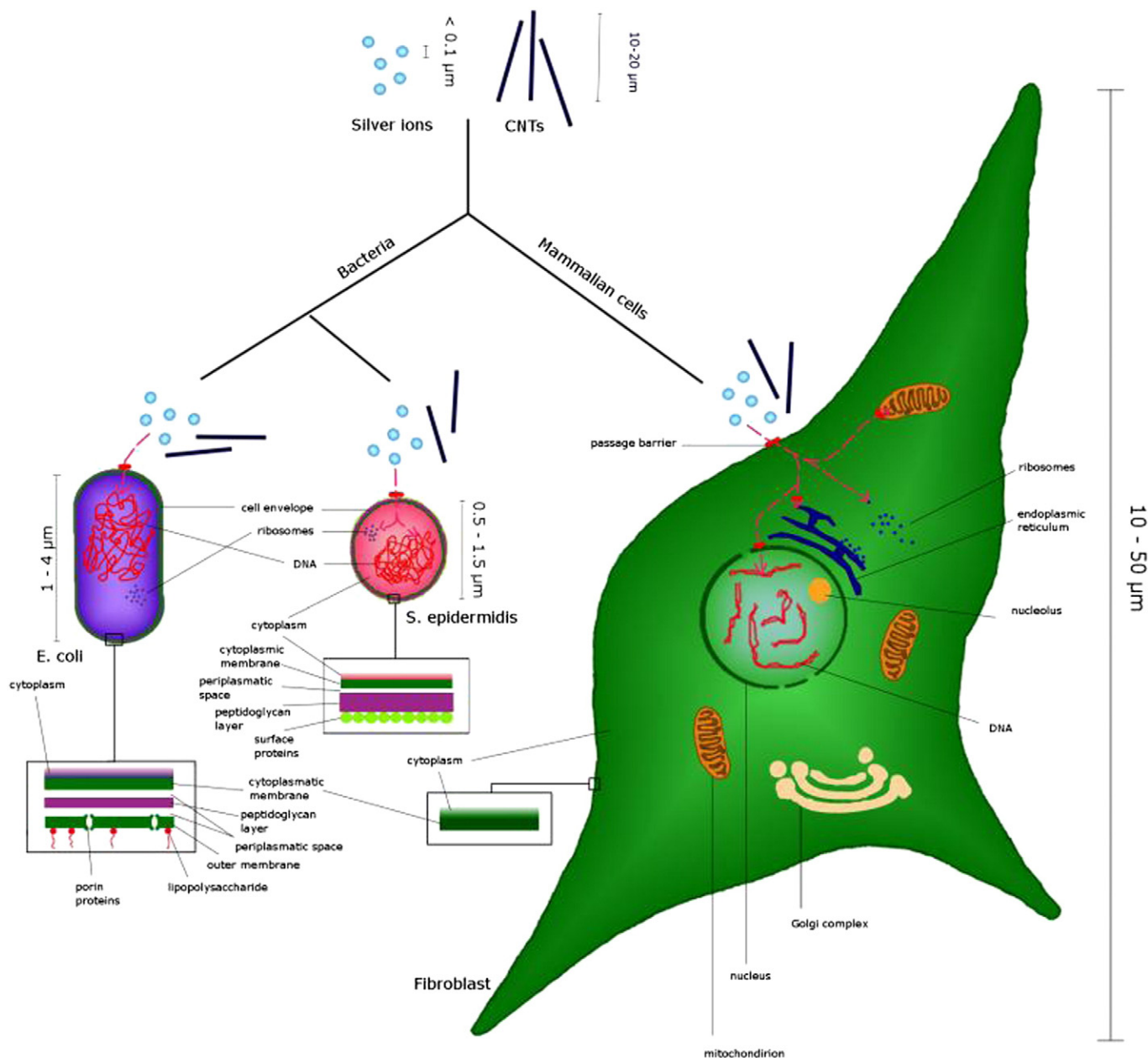


Fig. 11. Variation of density of L929 mouse fibroblast cells, *S. epidermidis* and *E. coli* with silver content. The rectangular box shows silver content for optimized biological properties.

Special attention has to be drawn on the influence of silver ions on human cells. Micrometer sized silver particles as well as silver nitrate or lactates are reported to show a strong cytotoxic effect which questions the application of silver in biocomposites [64]. However, recent studies including this research demonstrate retention of cytocompatibility upon addition of low amounts of silver nanoparticles (AgNPs) [63,65]. Also, silver ions can act as catalytic agents in the oxidation reactions, which form disulphide bonds (R–S–S–R), which affects the shape and function of the enzymes [5,59,66]. Compared to the bacterial behavior, the fibroblast adherence upon CNT addition is enhanced and the effects of silver addition are relatively low. Especially the results for 1 and 2 wt.% of Ag support the assumption that a low concentration of silver nanoparticles does not severely hamper the mammalian cell metabolism. Fig. 12 gives a plausible explanation for the differing modes of response compared to bacterial cells. First, mammalian cells are 10–100 times bigger than bacterial cells. For example a fibroblast cell has a diameter of 10–50  $\mu\text{m}$ , whereas *S. epidermidis* cells have a diameter of 0.5–1.5  $\mu\text{m}$ . Such a difference initiates completely different starting points for attacking silver ions, since the selective silver concentration in relation to the surface area is significantly lower (for bigger cells). Further, the compartmentalization (like the core, mitochondria, endoplasmic reticulum etc.) can have a protective effect, because the different membranes from compartments serve as additional passage barriers before Ag<sup>+</sup> ions can interact and form complexes. Hence, spatial partitioning of essential cell-functions keeps the fibroblast cell well protected against silver ion intrusion, and therefore can survive higher amounts of silver nanoparticles on its surface. Such existence of a “therapeutic window” to retain mammalian cell viability while eliciting bactericidal property has been confirmed by Steinrucke et al. [63]. Accordingly, based on current observations of retained mammalian cell viability and concomitant strong diminution of bacterial adherence in HA–ACNT–Ag composites indicate optimum silver contents between 2 and 10 wt.% (depending upon the compromise between the toughening and cytocompatibility).

### 3.5. Hardness and fracture toughness of HA–CNT–Ag biocomposites

The results of the Vickers indentation are reported in Table 2. An increase of the hardness upon CNT addition of up to 104% can be concluded as pure HA (C0A0) has a hardness value of 1.18 GPa whereas the CNT-reinforced samples show values from 1.20 GPa (C4A2) to 2.41 GPa (C4A1). Addition of silver nanoparticles do not show any traceable influence on the hardness. The maximum hardness is obtained for HA with 1% Ag and 4% CNT reinforcement. In order to evaluate fracture toughness, theoretical Young's modulus is estimated using the rule of



*Denaturing of DNA and binding of Ag<sup>+</sup> with thiol groups of enzymes lead to bacteria death*

*No deleterious effect on Mammalian Cell*

Fig. 12. Schematic of silver ions and CNTs intruding different cell types: *E. coli*, *S. epidermidis* and L929 fibroblast cells.

mixture eliciting that elastic modulus increases from 110 GPa for pure HA to values between 156.55 GPa and 159.12 GPa upon reinforcement with CNT and Ag (see Table 2). Further, the fracture toughness was calculated using Anstis' relation (Eq. (1)) using experimental observations of crack length under SEM as described in Section 2.3. The fracture toughness of the samples which are reinforced with CNT and Ag is observed to increase by 62%–243% as compared to pure hydroxyapatite from the value  $0.71 \text{ MPa m}^{1/2}$  to  $1.15 \text{ MPa m}^{1/2}$  (for C4A0) and up to  $2.44 \text{ MPa m}^{1/2}$  (for C4A10).

CNT pullout has been observed in fractured samples (Fig. 5) suggesting a strong interface of HA–CNT which is expected to increase the fracture toughness of the samples. Balani and Agarwal have suggested a few toughening mechanisms viz. CNT–splint interface sliding, CNT pinning (Slack-anchor), coating on CNT, nano-matrix–CNT friction,

CNT swording, CNT bending, CNT curling and CNT–matrix sliding interactions [67]. Further, the fracture toughness of the samples is expected to increase with increasing silver content assuming that higher volume fractions of silver will result in greater absorption of energy due to deformation of silver nanoparticles on absorbing energy during crack propagation, i.e. via crack tip selection, crack tip blunting and crack bridging.

The theoretical fracture toughness values  $K_{IC}^{\text{theoretical}}$  are thus directly related to the respective moduli and volume fractions of Ag nanoparticles and CNTs. According to Griffith theory of fracture, the contribution of interface energy in toughening is  $K_{IC} = \sqrt{(2E\gamma_s)}$  where  $\gamma_s$  is the interface energy of the cracked surface. The CNT–Ag, Ag–Ag and CNT–CNT interfaces are ignored as they are present in meager fractions compared to HA–HA, HA–Ag and HA–CNT interfaces. Considering

**Table 2**  
Evaluation of hardness, and fracture toughness.

Sample	Hardness H (GPa)	E/H	Fracture toughness $K_{IC}$ (MPa m <sup>1/2</sup> )
COA0	1.18 ± 0.04	93.2	0.71 ± 0.01
C4A0	1.91 ± 0.15	81.9	1.15 ± 0.03
C4A1	2.41 ± 0.35	65.0	1.36 ± 0.07
C4A2	1.20 ± 0.26	130.8	1.55 ± 0.05
C4A5	1.41 ± 0.17	111.9	2.10 ± 0.04
C4A10	1.78 ± 0.28	89.3	2.44 ± 0.04

the dependence of toughening on modulus of CNT and Ag along with contribution of interfacial energy, the theoretical value of fracture toughness is proposed as follows in Eq. (2).

$$K_{IC \text{ theoretical}} = \left\{ K_{IC}^{COA0} - (2E\gamma_{sCOA0}^{HA-HA})^{1/2} * 1 + V_f^{HA} * (2E\gamma_{sC4Ax}^{HA-HA})^{1/2} \right\} + \left\{ V_f^{Ag} * \left( (2E\gamma_{sC4Ax}^{HA-Ag})^{1/2} - A * E_{Ag} \right) \right\} + \left\{ V_f^{CNT} * \left( (2E\gamma_{sC4Ax}^{HA-CNT})^{1/2} - B * E_{CNT} \right) \right\} \quad (2)$$

where A and B are constants,  $V_f^{Ag}$  and  $V_f^{CNT}$  are the volume fractions of Ag nanoparticles and CNTs in C4Ax respectively,  $E_{Ag}$  and  $E_{CNT}$  are the modulus values of Ag nanoparticles and CNTs respectively, E is the modulus of the sample and  $\gamma_s$  is the interface energy which is taken to be 1.5–22 J/m<sup>2</sup> [68] for HA–CNT interface, 10 J/m<sup>2</sup> [69] for HA–Ag interface and 1 J/m<sup>2</sup> [69] for HA–HA interface.

**Table 3**  
Comparison of modeled values of fracture toughness with the experimental values.

Sample	$V_f^{HA}$	$V_f^{CNT}$	$V_f^{Ag}$	$A_{1/2}$ $\mu\text{m}$	$B_{1/2}$ $\mu\text{m}$	$K_{IC \text{ theoretical}}$ MPa m <sup>1/2</sup>	$K_{IC \text{ experimental}}$ MPa m <sup>1/2</sup>	Comments
COA0	1.000	0.000	0.000	0.031–0.119	0.241	–	0.71 ± 0.01	Base
C4A0	0.941	0.059	0.000	0.031–0.119	0.241	1.12–2.17	1.15 ± 0.03	In range
C4A1	0.938	0.059	0.003	0.031–0.119	0.241	1.17–2.23	1.36 ± 0.07	In range
C4A2	0.934	0.060	0.006	0.031–0.119	0.241	1.22–2.29	1.55 ± 0.05	In range
C4A5	0.924	0.061	0.015	0.031–0.119	0.241	1.38–2.49	2.10 ± 0.04	In range
C4A10	0.905	0.063	0.032	0.031–0.119	0.241	1.67–2.83	2.44 ± 0.04	In range

From the base fracture toughness of HA–20 vol.% Ag ( $COA20_{vol}$ ) determined by Asmus et al. [69], fracture toughness of HA–4 wt.% CNT calculated by Rishabh et al. [70] via fractal model, and the experimental fracture toughness obtained for pure HA ( $COA0$ ) and  $COAx$  samples, the values of the constants A and B were evaluated using Eq. (2). Then, using the constants A and B, the theoretical values of fracture toughness of all the samples were calculated and are presented in Table 3.

There are two points to be realized here: (i) the rate of increase of fracture toughness with CNT addition is higher (Fig. 13), since change in CNT reinforcement is lower (from 0.059 to 0.063 as elicited in Table 3), whereas increase in Ag is higher (from 0.000 to 0.032), and (ii) the degree of toughening with similar volume fraction is elicited by comparative contributions (lower values of constant A, when compared to higher values of constant B). It must be noted that low A value (between 0.031 and 0.119) indicates the good interfacing between Ag and HA matrix, when compared to high B value (of 0.241 listed in Table 3) indicating comparatively poor interface of CNT with HA matrix (because of negative contribution by constants A and B as shown in Eq. (2)). Since the toughening in CNT arises due to well known phenomena of CNT crack-bridging, crack deflection and CNT pullout, it is realized that CNT interfacial delamination leading to these toughening mechanisms is feeble (higher B value) when compared to volumetric toughening rendered by silver reinforcement (lower A value). Such a contribution is also confirmed through delineation of contributing toughening effects by isolated reinforcements (CNTs and Ag).

Fig. 13 shows a comparative feel of the reinforcing effects, where a direct jump of fracture toughness from 0.71 to 1.15 MPa m<sup>1/2</sup> is

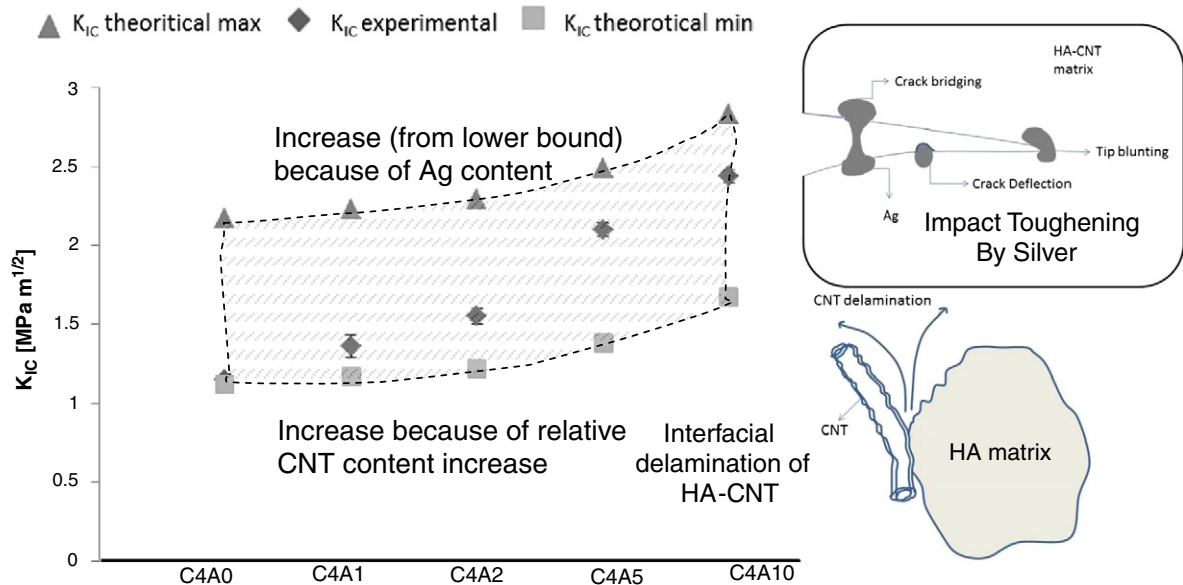


**Fig. 13.** Graph showing the experimental values of fracture toughness within the range of theoretical values predicted by model. Schematics showing the toughening mechanisms of Ag and CNT.

attributed to 4 wt.% CNT reinforcement (Table 2). Though CNT is kept at 4 wt.%, the addition of Ag (which possesses higher density) marginally raises the volume fraction of CNTs (see Table 3). Thus, the base line shows only a marginal positive slope (i.e. increasing fracture toughness with increasing CNT content). On the other hand, the increase of fracture toughness with silver addition shows a further jump from 1.15 to 1.36 MPa m<sup>1/2</sup>, with 1 wt.% Ag addition. But with half the volume fraction (of ~0.32 for 10 wt.% Ag reinforcement) shows that fracture toughness rises to 2.44 MPa m<sup>1/2</sup> (3.43 times that of pure HA) when compared to that of CNT reinforcement (vol. fraction of 0.60, eliciting only 1.62 times the fracture toughness). Thus, it can be claimed that the volumetric toughening mechanisms of Ag dominate over interfacial strengthening contributed by CNT for enhanced fracture toughness of HA–CNT–Ag composites. It must also be realized that a minimum fracture toughness of 2 MPa m<sup>1/2</sup> is required [5] for application as potential bone implant, which makes C4A5 and C4A10 as potential HA–CNT–Ag biocomposites for bone-replacement.

#### 4. Conclusions

HA–CNT–Ag samples were successfully spark plasma sintered and resulted as highly dense pellets (~95%). Phase analysis revealed the retention of hydroxyapatite, silver, and CNTs, which have elicited dramatic fracture toughness enhancement of up to 244% (i.e. from 0.71 MPa m<sup>0.5</sup> of pure HA to 2.44 MPa m<sup>1/2</sup>) upon 4 wt.% CNT and 10 wt.% Ag reinforcement. CNT appears to have a bactericidal effect on Gram positive bacteria (*S. epidermidis* density decreased to about two thirds of that on pure HA) whereas it enhanced the proliferation of Gram negative bacteria (*E. coli* density increase by around 8.5%). The decrease of both, Gram positive and Gram negative bacteria upon increasing silver content can be confirmed. Cell culturing with L929 fibroblasts showed excellent biocompatibility of HA samples, CNT appears to enhance the cell attachment. Further, 5–10 wt.% of silver elicited ~75% cell density compared to that of pure HA along with a good fracture toughness (>2 MPa m<sup>1/2</sup>). Interfacial toughening with CNT reinforcement appeared to be shadowed by volumetric toughening by Ag reinforcement. Thus, 5–10 wt.% silver content in 4 wt.% CNT reinforced HA biocomposite shows promising mechanical as well as biological properties. Application of HA–CNT–Ag biocomposite is expected to work well as an outer layer of a functionally gradient material in combination with core materials of higher fracture toughness.

#### Acknowledgment

The authors thank Mr. Diwakar for assisting in Spark plasma sintering of the samples. Mr. Rajeev Sharma and Ms. Aditi Pandey are also acknowledged for their assistance in bacterial culture and cell culture experiments respectively. KB acknowledges MHRD for financial support. Authors thank Prof. Rajeev Gupta, IIT Kanpur, for assisting with Raman spectroscopy.

#### References

- [1] U. Heise, J.F. Osborn, F. Duwe, Hydroxyapatite ceramic as a bone substitute, *Int. Orthop.* 14 (1990) 329–338.
- [2] L.L. Hench, Bioceramics: from concept to clinic, *J. Am. Ceram. Soc.* 74 (1991) 1487–1510.
- [3] M. Jarcho, Calcium phosphate ceramics as hard tissue prosthetics, *Clin. Orthop. Relat. Res.* 157 (1981) 259–278.
- [4] A. Ganguli, C. Steward, S.L. Butler, G.J. Philips, S.T. Meikle, A.W. Lloyd, et al., Bacterial adhesion to bisphosphonate coated hydroxyapatite, *J. Mater. Sci. Mater. Med.* 16 (2005) 283–287.
- [5] M.A.F. Afzal, S. Kalmodia, P. Kesarwani, B. Basu, K. Balani, Bactericidal effect of silver-reinforced carbon nanotube and hydroxyapatite composites, *J. Biomater. Appl.* 27 (8) (2013) 967–978.
- [6] W. Suchanek, M. Yoshimura, Processing and properties of hydroxyapatite-based biomaterials for use as hard tissue replacement implants, *J. Mater. Res.* 13 (1998) 94–117.
- [7] G. Muralithran, S. Ramesh, The effects of sintering temperature on the properties of hydroxyapatite, *Ceram. Int.* 26 (2000) 221–230.
- [8] K. Balani, R. Anderson, T. Laha, M. Andara, J. Tercero, E. Crumpler, A. Agarwal, Plasma-sprayed carbon nanotube reinforced hydroxyapatite coatings and their interaction with human osteoblasts in vitro, *Biomaterials* 28 (2007) 618.
- [9] T. Akasaka, F. Watari, Y. Sato, K. Tohji, Apatite formation on carbon nanotubes, *Mater. Sci. Eng. C* 26 (2006) 675–678.
- [10] S. Kalmodia, S. Goenka, T. Laha, D. Lahiri, B. Basu, K. Balani, Microstructure, mechanical properties, and in vitro biocompatibility of spark plasma sintered hydroxyapatite–aluminum oxide–carbon nanotube composite, *Mater. Sci. Eng. C* 30 (2010) 1162–1169.
- [11] J.L. Xu, K.A. Khor, J.J. Sui, W.N. Chen, Preparation and characterization of a novel hydroxyapatite/carbon nanotubes composite and its interaction with osteoblast-like cells, *Mater. Sci. Eng. C* 29 (2009) 44.
- [12] D. Lahiri, S. Ghosh, A. Agarwal, Carbon nanotube reinforced hydroxyapatite composite for orthopedic application: a review, *Mater. Sci. Eng. C* 32 (2012) 1727–1758.
- [13] J. Chlopek, B. Czajkowska, B. Szaraniec, E. Frackowiak, K. Szostak, F. Beguin, In vitro studies of carbon nanotubes biocompatibility, *Carbon* 44 (2006) 1106.
- [14] J. Tercero, S. Namin, D. Lahiri, K. Balani, N. Tsoukias, A. Agarwal, Effect of carbon nanotube and aluminum oxide addition on plasma-sprayed hydroxyapatite coating's mechanical properties and biocompatibility, *Mater. Sci. Eng. C* 29 (2009) 2195.
- [15] K.L. Elias, R.L. Price, T.J. Webster, Enhanced functions of osteoblasts on nanometer diameter carbon fibers, *Biomaterials* 23 (2002) 3279–3287.
- [16] K. Balani, Y. Chen, S.P. Harimkar, N.B. Dahotre, A. Agarwal, Tribological behavior of plasma-sprayed carbon nanotube-reinforced hydroxyapatite coating in physiological solution, *Acta Biomater.* 3 (2007) 944–951.
- [17] L.P. Zanello, B. Zhao, H. Hu, R.C. Haddon, Bone Cell Proliferation on Carbon Nanotubes, *Nano Lett.* 6 (3) (2006) 562–567.
- [18] K.H. Park, M. Chhowalla, Z. Iqbal, F. Sesti, Single-walled Carbon Nanotubes Are a New Class of Ion Channel Blockers, *J. Biol. Chem.* 278 (2003) 50212.
- [19] F. Watari, T. Akasaka, K. Ishikawa, M. Matsuoka, E. Hirata, N. Terada, A. Yokoyama, M. Uo, S. Itoh, Y. Yawaka, M. Suzuki, N. Takashi, Y. Totsuka, Y. Kitagawa, S. Abe, I.D. Rosca, Y. Kuboki, Y. Bando, Various nanotube scaffolds for cell proliferation, *Mater. Sci. Forum* 631–632 (2010) 181–186.
- [20] A. Shvedova, V. Castranova, E. Kisin, D. Schwegler-Berry, A. Murray, V. Gandelman, et al., Exposure to carbon nanotube material: assessment of nanotube cytotoxicity using human keratinocyte cells, *J. Toxicol. Environ. Health A* 66 (2003) 1909–1926.
- [21] D.X. Cui, F.R. Tian, C.S. Ozkan, M. Wang, H.J. Gao, Effect of single wall carbon nanotubes on human HEK293 cells, *Toxicol. Lett.* 55 (2005) 73.
- [22] P. Cherukuri, S.M. Bachilo, S.H. Litovsky, R.B. Weisman, Near-infrared fluorescence microscopy of singlewalled carbon nanotubes in phagocytic cells, *J. Am. Chem. Soc.* 126 (2004) 15638–15639.
- [23] S. Kang, M. Herzberg, D.F. Rodrigues, M. Elimelech, Antibacterial Effects of Carbon Nanotubes: Size Does Matter! *Langmuir* 24 (2008) 6409–6413.
- [24] R. Narayan, C.J. Berry, R.L. Brignon, Structural and biological properties of carbon nanotube composite films, *Mater. Sci. Eng. B* 123 (2005) 123–129.
- [25] Y. Bai, I.S. Park, S.J. Lee, T.S. Bae, F. Watari, M. Uo, M.H. Lee, Aqueous dispersion of surfactant-modified multiwalled carbon nanotubes and their application as an antibacterial agent, *Carbon* 49 (2011) 3663–3671.
- [26] Q. Ling Feng, T. Nam Kim, J. Wu, E. Seo Park, J. Ock Kim, D. Young Lim, et al., Antibacterial effects of Ag–HA thin films on alumina substrates, *Thin Solid Films* 335 (1998) 214–219.
- [27] S. Nath, S. Kalmodia, B. Basu, Densification, phase stability and in vitro biocompatibility property of hydroxyapatite – 10 wt. % silver composites, *J. Mater. Sci. Mater. Med.* 21 (2010) 1273–1287.
- [28] N. Saha, K. Keskinbora, E. Suvaci, B. Basu, Sintering, microstructure, mechanical, and antimicrobial properties of HA–ZnO biocomposites, *J. Biomed. Mater. Res. B* 95B (2010) 430–440.
- [29] U. Klueh, V. Wagner, S. Kelly, A. Johnson, J.D. Bryers, Efficacy of silver-coated fabric to prevent bacterial colonization and subsequent device-based biofilm formation, *J. Biomed. Mater. Res.* 53 (2000) 621–631.
- [30] W. Ghandour, J.A. Hubbard, J. Deistrung, M.N. Hughes, R.K. Poole, The uptake of silver ions by *Escherichia coli*: toxic effects and interactions with copper ions, *Appl. Microbiol. Biotechnol.* 28 (1988) 559–565.
- [31] H.G. Petering, Pharmacology and toxicology of heavy metals: silver, *Pharmacol. Ther.* A 1 (1976) 127–130.
- [32] W.J. Schreurs, H. Rosenberg, Effect of silver ions on transport and retention of phosphate by *Escherichia coli*, *J. Bacteriol.* 152 (1982) 7–13.
- [33] V. Alt, T. Bechert, P. Steinrucke, M. Wagener, P. Seidel, E. Dingeldein, E. Domann, R. Schnettler, An in vitro assessment of the antibacterial properties and cytotoxicity of nanoparticulate silver bone cement, *Biomaterials* 25 (2004) 4383–4391.
- [34] C. Baldi, C. Minoia, A. Di Nucci, E. Capodaglio, L. Manzo, Effects of silver in isolated rat hepatocytes, *Toxicol. Lett.* 41 (1988) 261–268.
- [35] P.V. AshaRani, G. Low Kah Mun, M. Prakash Hande, S. Valiyaveetil, Cytotoxicity and Genotoxicity of Silver Nanoparticles in Human Cells, *Am. Chem. Soc.* 3 (2) (2009) 279–290.
- [36] Z.A. Munir, U. Anselmi-Tamburini, The effect of electric field and pressure on the synthesis and consolidation of materials: A review of the spark plasma sintering method, *J. Mater. Sci.* 41 (2006) 763–777.
- [37] U. Anselmi-Tamburini, J.E. Garay, Z.A. Munir, A. Tacca, F. Maglia, G. Spinolo, Spark plasma sintering and characterization of bulk nanostructured fully stabilized zirconia: Part II. Characterization studies, *J. Mater. Res.* 19 (2004) 3255.
- [38] V. Viswanathan, T. Laha, K. Balani, A. Agarwal, S. Seal, Challenges and advances in nanocomposite processing techniques, *Mater. Sci. Eng. R* 54 (2006) 121–285.
- [39] Z. Evis, R.H. Doremus, Hot-pressed hydroxylapatite/monoclinic zirconia composites with improved mechanical properties, *J. Mater. Sci.* 42 (2007) 2426–2431.
- [40] B. Wei, J. Zhang, J. Liang, D. Wu, The mechanism of phase transformation from carbon nanotube to diamond, *Carbon* 36 (1998) 997–1001.

- [41] J. Shen, F. Zhang, J.F. Sun, Y.Q. Zhu, D.G. McCartney, Spark plasma sintering assisted diamond formation from carbon nanotubes at very low pressure, *Nanotechnology* 17 (2006) 2187–2191.
- [42] J.L. Li, L.J. Wang, T. He, W. Jiang, Surface graphitization and mechanical properties of hot-pressed bulk carbon nanotubes compacted by spark plasma sintering, *Carbon* 45 (2007) 2636–2642.
- [43] Y.Y. Zhang, C.M. Wang, V.B.C. Tan, Buckling of carbon nanotubes at high temperatures, *Nanotechnology* 20 (2009) 215702.
- [44] M.A.F. Afzal, P. Kesarwani, K.M. Reddy, S. Kalmodia, B. Basu, K. Balani, Functionally graded hydroxyapatite–alumina–zirconia biocomposite: Synergy of toughness and biocompatibility, *Mater. Sci. Eng. C* 32 (2012) 1164–1173.
- [45] H. Guoa, K. Aik Khorb, Y. Chiang Boeya, X. Miaoa, Laminated and functionally graded hydroxyapatite/yttria stabilized tetragonal zirconia composites fabricated by spark plasma sintering, *Biomaterials* 24 (2003) 667–675.
- [46] F. Erdogan, *Fracture Mechanics of Functionally Graded Materials*, *Compos. Eng.* 5 (7) (1995) 753–770.
- [47] F. Wataria, A. Yokoyamaa, M. Omorib, T. Hiraic, M. Uoa Hideomi Kondoa, T. Kawasakia, Biocompatibility of materials and development to functionally graded implant for bio-medical application, *Compos. Sci. Technol.* 64 (2004) 893–908.
- [48] T. Kunzler, T. Drobek, M. Schuler, N. Spencer, Systematic study of osteoblast and fibroblast response to roughness by means of surface-morphology gradients, *Biomaterials* 28 (2007) 2175–2182.
- [49] B.R. Lawn, G.R. Anstis, P. Chantikul, D.B. Marshall, A critical evaluation of indentation techniques for measuring fracture toughness: I, direct crack measurements, *J. Am. Ceram. Soc.* 64 (1981) 533–538.
- [50] B. Lukic, J.W. Seo, E. Couteau, K. Lee, S. Gradecak, R. Berkecz, K. Hernadi, S. Delpeux, T. Cacciaguerra, F. Beguin, A. Fonseca, J.B. Nagy, G. Csanyi, A. Kis, A.J. Kulik, L. Forro, Elastic modulus of multi-walled carbon nanotubes produced by catalytic chemical vapour deposition, *Appl. Phys. A* 80 (2005) 695–700.
- [51] V. Sergo, O. Sbaizero, D. Clarke, Mechanical and chemical consequences of the residual stresses in plasma sprayed hydroxyapatite coatings, *Biomaterials* 18 (2009) 477–482.
- [52] M.A. Walters, Y.C. Lang, N.C. Blumenthal, R.Z. LeGeros, I.L.A. Konsker, A Raman and Infrared Spectroscopic Investigation of Biological Hydroxyapatite, *J. Inorg. Biochem.* 39 (1990) 193–200.
- [53] E.F. Antunes, A.O. Lobo, E.J. Corat, V.J. Trava-Airoldi, A.A. Martin, C. Verissimo, Comparative study of first- and second-order Raman spectra of MWCNT at visible and infrared laser excitation, *Carbon* 44 (2006) 2202–2211.
- [54] L. Wang, X. Wang, L. Wang, L. Zhang, Field emission characteristics of nanostructured carbon films deposited on differently pretreated Mo films, *Appl. Surf. Sci.* 255 (2008) 3257–3262.
- [55] I. Lahiri, D. Lahiri, S. Jin, A. Agarwal, W. Choi, Carbon Nanotubes: How Strong Is Their Bond with the Substrate? *ACS Nano* 5 (2) (2011) 780–787.
- [56] K. Balani, S. Harimkar, A. Keshri, Y. Chen, N. Dahotre, A. Agarwal, Multiscale wear of plasma-sprayed carbon-nanotube-reinforced aluminum oxide nanocomposite coating, *Acta Mater.* 56 (2008) 5984–5994.
- [57] G.T. Coupin, C.D. Muller, A. Remy-Kristensen, J.G. Kuhry, Cell surface membrane homeostasis and intracellular membrane traffic balance in mouse L929 cells, *J. Cell Sci.* 112 (1999) 2431–2440.
- [58] G.T. Coupin, C.D. Muller, A. Remy-Kristensen, J.G. Kuhry, Cell surface membrane homeostasis and intracellular membrane traffic balance in mouse L929 cells, *J. Cell Sci.* 112 (1999) 2431–2440.
- [59] S. Kelly, A. Johnson, U. Klueh, V. Wagner, J.D. Bryers, Efficacy of silver-coated fabric to prevent bacterial colonization and subsequent device-based biofilm formation, *J. Biomed. Mater. Res.* 53 (2000) 621–631.
- [60] J. Deistrung, M.N. Hughes, R.K. Poole, W. Ghandour, J.A. Hubbard, The uptake of silver ions by *Escherichia coli*: toxic effects and interactions with copper ions, *Appl. Microbiol. Biotechnol.* 28 (1988) 559–565.
- [61] H.G. Petering, Pharmacology and toxicology of heavy metals: silver, *Pharmacol. Ther.* A 1 (1976) 127–130.
- [62] H. Rosenberg, W.J. Schreurs, Effect of silver ions on transport and retention of phosphate by *Escherichia coli*, *J. Bacteriol.* 152 (1982) 7–13.
- [63] P. Steinrucke, M. Wagener-P Seidel, E. Dingeldein, E. Domann, R. Schnettler, V. Alt, T. Bechert, An in vitro assessment of the antibacterial properties and cytotoxicity of nanoparticulate silver bone cement, *Biomaterials* 25 (2004) 4383–4391.
- [64] A. Di Nucci, E. Capodaglio, C. Baldi, C. Minoia, L. Manzo, Effects of silver in isolated rat hepatocytes, *Toxicol. Lett.* 41 (1988) 261–268.
- [65] S. Kalmodia, S. Nath, B. Basu, Densification, phase stability and in vitro biocompatibility property of hydroxyapatite - 10 wt, *J. Mater. Sci. Mater. Med.* 21 (2010) 1273–1287.
- [66] R.L. Davies, S.F. Etris, The development and functions of silver in water purification and disease control, *Catal. Today* 36 (1997) 107–114.
- [67] K. Balani, A. Agarwal, Damping behavior of carbon nanotube reinforced aluminum oxide coatings by nanomechanical dynamic modulus mapping, *J. Appl. Phys.* 104 (2008) 063517.
- [68] D. Lahiri, V. Singh, A.K. Keshri, S. Seal, A. Agarwal, Carbon nanotube toughened hydroxyapatite by spark plasma sintering: Microstructural evolution and multiscale tribological properties, *Carbon* 48 (2010) 3103–3120.
- [69] S.M.F. Asmus, S. Sakakura, G. Pezzotti, Hydroxyapatite Toughened by Silver Inclusions, *J. Compos. Mater.* 37 (2003) 2117–2129.
- [70] A. Rishabh, M.R. Joshi, K. Balani, Fractal model for estimating fracture toughness of carbon nanotube reinforced aluminium oxide, *J. Appl. Phys.* 107 (2010) 123532.